IMAGE ENHANCEMENT USING MULTISCALE DIFFERENTIAL OPERATORS

Yu-Ping Wang[†], *Qiang Wu*[‡], *Kenneth R. Castleman*[‡], *and Zixiang Xiong*[†]

[†]Dept of Electrical Engineering, Texas A&M University, College Station, TX 77843
[‡]The Advanced Digital Imaging Research, LLC. 2525 S. Shore Blvd., #100, League city, TX 77573

ABSTRACT

Differential operators have been widely used for multiscale geometric descriptions of images. Efficient computation of these differential operators can be obtained by taking advantage of the spline techniques. In this paper, we make use of a special class of these operators for image enhancement, with a particular application to chromosome image enhancement. These operators constitute a translation invariant wavelet transform well suited for the structural description of chromosome geometry. Based on the fact that the geometrical features like edges are correlated between different scales in the representation, a novel algorithm is designed to enhance the salient features of the image. Comparisons of this algorithm with other approaches are presented.

1. INTRODUCTION

The geometry of images is usually characterized using differential or difference operators such as the gradient operator, Laplacian operator and compass operator [1]. It is well known from both psychophysical and physiological experiments that edges of images are captured in the visual context of mammals at different resolution levels. A class of wavelets for multiscale differential representations of images was proposed in [2, 3].

The objective of image enhancement is to improve the visibility of low-contrast features while suppressing the noise. Among various enhancement methods, sharpening techniques are usually designed by using gradient information derived from the Sobel operator, Roberts operator, or the compass operator. The adaptive enhancement method, exploiting the first derivative, has been used for mammographic image enhancement [4]. Since differential operators can be regarded as high pass filters, these techniques actually sharpen the image by extrapolation of its high frequency information. The Laplacian pyramid, as one of its variants, has also been used for image enhancement [5].

Motivated by both the close approximations of B-spline bases to the Gaussian and the wavelet theory, Wang et. al. provide a more formal framework for multiscale representations using differential operators in [2, 3, 6]. By taking advantage of the spline properties, fast algorithms are derived. Moreover, these representations are different from the usual wavelet models in that they are translation-invariant. As shown in [7], thresholding in the translation invariant wavelet domain eliminates some of the unpleasant artifacts introduced by modification of orthogonal wavelet expansion coefficients. Therefore, these over-complete representations provide more flexibility, and they outperform the orthogonal bases. They are very suitable for geometric-based processing.

This paper makes use of these differential representations for image enhancement applications by exploiting the geometric correlation of image features in these domains. The resulting enhancement scheme is particularly applied to chromosome image enhancement.

Q. Wu and K. Castleman's work is supported by the NIH under the SBIR Grant 5 R44 HD33658-03 and Y. Wang and Z. Xiong's work is supported in part by the NSF under the career grant 0096070, the ARO under the YIP grant DAAD19-00-1-0509, and a gift grant from ADIR.

2. MULTIRESOLUTION DIFFERENTIAL REPRESENTATIONS OF IMAGES

A family of wavelets was designed in [3] which are the derivatives of splines. An image can be synthesized from its derivative components at multiple scales. These differential operators include the gradient operator, the Laplacian, the second derivative operator and multi-directional operators. At each scale, these operators resemble the Sobel, Roberts and compass operators. In this section, we review the main results for the second derivative operator case, which is used in this paper. More details can be found in [2, 3].

2.1. Decomposition and reconstruction of an image from its directional derivative components

The multiscale smoothing of images is obtained by convolution of images with the 2-D B-spline function defined as $\beta^n(x,y) = \beta^n(x)\beta^n(y)$ at different scales, where n is the order of B-spline. After taking the second directional derivative of the smoothed image $f * \beta^n_{2^j}(x,y)$ along the gradient orientations, the three directional derivative components, or wavelet transforms, are given by

$$\begin{aligned} W^1_{2^j} f(x,y) &= \frac{\partial^2 (f * \beta^n_{2^j}(x,y))}{\partial x^2}, \\ W^2_{2^j} f(x,y) &= \frac{\partial^2 (f * \beta^n_{2^j}(x,y))}{\partial y^2}, \\ W^3_{2^j} f(x,y) &= \frac{\partial^2 (f * \beta^n_{2^j}(x,y))}{\partial x \partial y} \end{aligned} \tag{1}$$

By taking advantage of the refinable properties of splines, we can obtain a recursive algorithm for the computations of these three local partial derivative components along the dyadic scales $\{2^j\}_{j\in Z}$ [3]. Alternatively, we have the following **discrete decomposition formula**:

$$\begin{cases} S_{2^j} f &= S_{2^{j-1}} f * (h,h)_{\uparrow 2^{j-1}} \\ W^1_{2^j} f &= S_{2^{j-1}} f * (g^{(2)}, d)_{\uparrow 2^{j-1}} \\ W^2_{2^j} f &= S_{2^{j-1}} f * (d, g^{(2)})_{\uparrow 2^{j-1}} \\ W^3_{2^j} f &= S_{2^{j-1}} f * (g^{(1)}, g^{(1)})_{\uparrow 2^{j-1}} \end{cases} \tag{2}$$

where $I * (h,g)_{\uparrow 2^{j-1}}$ represents the separable convolution of the rows and columns of the image with the 1-D filters $[h]_{\uparrow 2^{j-1}}$ and

$[g]_{\uparrow 2^{j-1}}$ respectively. The symbol d denotes the Dirac filter whose impulse is 1 at the origin and 0 elsewhere. The up-sampling operation of a sequence $\{h(n)\}$ by an integer multiple m is defined as $[h]_{\uparrow m}$. $\{h\}$ are the binomial filters. $\{g^{(1)}\}$, $\{g^{(2)}\}$ are the first and second order difference operators.

Under the perfect reconstruction condition, an image can be reconstructed from its wavelets components (2) using the following **discrete reconstruction formula**:

$$S_{2^{j-1}}f = W^1_{2^j}f * (\tilde{g}^{(2)}, u)_{\uparrow 2^{j-1}} + W^2_{2^j}f * (u, \tilde{g}^{(2)})_{\uparrow 2^{j-1}} + W^3_{2^j}f * (\tilde{g}^{(1)}, \tilde{g}^{(1)})_{\uparrow 2^{j-1}} + S_{2^j}f * (\tilde{h}, \tilde{h})_{\uparrow 2^{j-1}}, \quad (3)$$

where $u(j) = \frac{1}{2^{2n+2}}\binom{2n+2}{j}, 0 \le j \le 2n+2$, are the FIRs of the transfer function $U(\omega) = H^2(\omega)$. $\{\tilde{g}^{(1)}\}$ and $\{\tilde{g}^{(2)}\}$ are the reconstruction filters corresponding to $\{g^{(1)}\}$ and $\{g^{(2)}\}$ respectively.

It can be further verified that an image $f(x, y)$ can be recovered from its three directional derivative components $\{W^k_{2^j}\}^{k=1,2,3}_{j\in Z}$ in the continuous form as

$$f(x, y) = \sum_{j=-\infty}^{\infty} (W^1_{2^j}f * \chi^{n,1}(x, y) + W^2_{2^j}f * \chi^{n,2}(x, y) + W^3_{2^j}f * \chi^{n,3}(x, y)). \quad (4)$$

where $\chi^{n,1}, \chi^{n,2}$ and $\chi^{n,3}$ are the 3 reconstruction filters along horizontal, vertical and diagonal directions respectively.

2.2. Discrete filters for both decomposition and reconstruction

We only give all the filters for both decomposition and reconstruction in the above formula in the case of $n = 3$, as shown in table 1. The derivation of these filters and general formulas for any order of splines could be found in [3].

taps	h	$\tilde{h}$	$g^{(1)}$	$g^{(2)}$	$\tilde{g}^{(1)}$	$\tilde{g}^{(2)}$	u
-4	0	0	0	0	$\frac{1}{256}$	0	$\frac{1}{256}$
-3	0	0	0	0	$\frac{9}{256}$	$\frac{-1}{128}$	$\frac{8}{256}$
-2	$\frac{1}{16}$	$\frac{1}{16}$	0	0	$\frac{37}{256}$	$\frac{-10}{128}$	$\frac{28}{256}$
-1	$\frac{1}{4}$	$\frac{1}{4}$	-1	1	$\frac{93}{256}$	$\frac{-47}{128}$	$\frac{56}{256}$
0	$\frac{3}{8}$	$\frac{3}{8}$	1	-2	$\frac{-93}{256}$	$\frac{140}{128}$	$\frac{70}{256}$
1	$\frac{1}{4}$	$\frac{1}{4}$	0	1	$\frac{-37}{256}$	$\frac{-47}{128}$	$\frac{56}{256}$
2	$\frac{1}{16}$	$\frac{1}{16}$	0	0	$\frac{-9}{256}$	$\frac{-10}{128}$	$\frac{28}{256}$
3	0	0	0	0	$\frac{-1}{256}$	$\frac{-1}{128}$	$\frac{8}{256}$
4	0	0	0	0	0	0	$\frac{1}{256}$

Table 1. Filters of both decomposition and reconstructions for cubic splines.

2.3. Fast and parallel implementation

Since all the filters $\{h^{(j)}\}, \{g^{(j)}\}$ are linear combinations of binomials, the computational efficiency can be further improved using the *Pascal triangular algorithm* [3]. In detail, due to the following identity

$$\binom{n}{k} = \binom{n-1}{k} + \binom{n-1}{k-1}$$

the convolution with a nth binomial can be realized using only *addition* operations recursively from the 0th binomial (unit impulse). The last normalization factor $\frac{1}{2^{n+1}}$ can be implemented directly by *bit shift* operation rather than multiplication. We can call this method the **moving average sum technology**, which leads to an easy hardware realization. The complexity of the approach is $\mathcal{O}(N)$, and hence an improvement over the recursive algorithms (2) and (3) which have complexity $\mathcal{O}(N log_2 N)$. In addition, it is easy to show that these filters allow integer implementation of these wavelet transforms.

As a result, one can accomplish a fast and parallel implementation of the dyadic wavelet transforms without resorting to the recursive pyramid-like algorithms. The smooth approximations $\{S_{2^j}\}_{1\le j\le J}$ and the wavelet transforms $\{W_{2^j}\}_{1\le j\le J}$ along different scales can be computed simultaneously and directly from the finest scale approximation, $S_{2^0}f$, using the following formula

$$\begin{cases} S_{2^j}f = S_{2^0}f * h^{(j)}, \\ W_{2^j}f = S_{2^0}f * g^{(j)}, \quad j = 1, 2, \cdots, J. \end{cases} \quad (5)$$

The binomial filter $\{h^{(j)}\}$ can be obtained easily from the following iterative relation

$$h^{(j)}[n] = \frac{1}{2^{n+1}} \sum_{l=0}^{n+1} \binom{n+1}{k} h^{(j-1)}[n - 2^{j-1}l], \quad n \in Z \quad (6)$$

and $\{g^{(j)}\}$ is obtained by taking the first or second order difference of the $\{h^{(j-1)}\}$ with a spacing 2^{j-1}.

3. ENHANCEMENT ALGORITHMS

3.1. The correlation across different scales

As edges exist across multiple scales, there must be some correlation across different scales [8]. Before the advent of wavelets, multiscale point-wise products (MPP) had been used to enhance the multiscale peaks due to edges while suppressing noise, by exploiting the multiscale correlation of the desired signal [9]. The MPP is defined by

$$p_K(n) = \prod_{j=1}^{K} W_{2^j}f(n) \quad (7)$$

where K is the maximum number of scales used for computing correlations. This criteria has been used for detection, localization [8] and filtering of magnetic resonance images [10]. An example is shown in Fig. 1. As maxima of $W_{2^j}f(n)$ due to edges in signal $f(n)$ tend to propagate across scales, whereas maxima due to noise do not, p_K will reinforce the signal response and not the noise. In [11] we have proved that the density of maxima, D_s, of white noise will follow the following formula:

$$D_s = \frac{\sqrt{3}}{2\pi}\frac{1}{s}\frac{1}{\sqrt{n+1}} \quad (8)$$

where s is the scale of smoothing and n is the order of spline. In other words, the number of local maxima due to noise decrease quickly with increasing scale due to increased smoothing. If we take dyadic scales, the average number of local maxima at $s = 2^{j+1}$ will be half of that at scale $s = 2^j$.

The statistics of p_K is characterized in [8]. The resulting probability density functions (pdf's) are generally non-Gaussian and heavy tailed. MPP could be used for detection and estimation of step change locations.

In the above discussion, we only deal with the one-dimensional case. For 2-D images, MPP should be sensitive to direction. For three different directions, the correlation quantity MPP is different along three different directions.

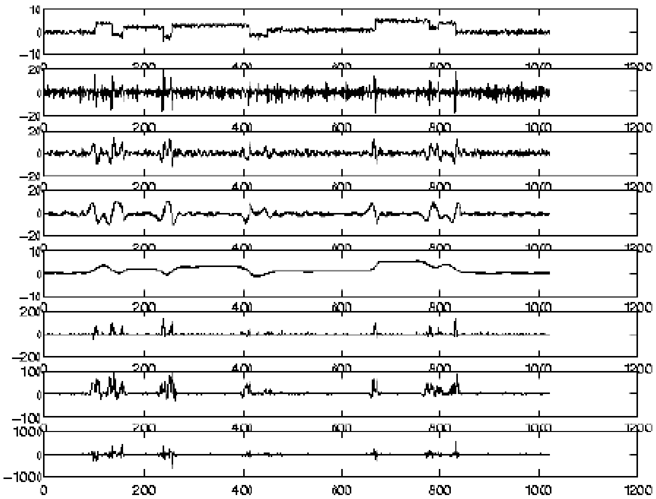

Fig. 1. Wavelet Decompositions of a simulated signal using cubic spline wavelets. Top row is the block signal added with white noise. From 2nd row to 4th row are the wavelet decomposition coefficients. 5th row is the smooth component. 6th row and 7th row are the multiscale point-wise products (MPP) between adjacent two scales. 8th row is the MPP among 3 scales.

3.2. The enhancement algorithm

Based on the above observation, we propose the following algorithm for edge enhancement in 2-D images.

1. Perform the multiscale differential decomposition of images using the spline wavelets. Thus we have a sequence of wavelet decompositions $\{W^d_{2^j} f, d = 1, 2, 3; 0 <= j <= J; S_{2^J} f\}$ along the horizontal, vertical and diagonal directions.

2. Sort the values of $p^d_K(n), d = 1, 2, 3$ at each pixel from low to high values and then normalize them to $[0, 1]$. Let the user set the threshold as μ. Then threshold and modify the images using the following formula:

$$\tilde{W}^d_{2^j} f(n) = \begin{cases} \lambda W^d_{2^j} f(n), & \text{if } p^d_K \geq \mu \\ 0, & \text{if } p^d_K < \mu \end{cases} \tag{9}$$

where λ is an adjustable constant. The low-frequency components of images $S_{2^J} f$ are kept unchanged.

3. Do the inverse wavelet transform using reconstruction formula (3) to get the enhanced images.

The choice of $\mu \in [0, 1]$ depends on the noise level of the image. Since the images we acquired for chromosome enhancement contain little noise, we usually set μ below 0.1. The main objective is contrast enhancement. The user has the option to input different value of λ for different degree of enhancement as he desires. An example result using the above algorithm is shown in Fig. 2. We choose $\lambda = 3.2$ and $\mu = 0.01$ for this figure as well as for other images used in the experiments.

4. RESULTS AND COMPARISONS

Common techniques for contrast enhancement generally can be categorized into two classes [5]. In the first one, techniques such as histogram equalization, modify the brightness of each pixel based on the statistical information of an image. In the second one, it separates the high and/or low-frequency components of images, manipulating them separately and re-combine them, for example, as in the unsharp masking method.

The quantitative measurement of the contrast improvement is often very difficult. Moreover, there is no universal standard for measuring both objective and subjective performance of the enhancement. The contrast is often defined as the difference in mean luminances between an object and its surroundings. There are many definitions of contrast measures. We adopt the measure proposed in [12] and the local contrast defined by the difference of mean values in two rectangular windows centered on a pixel. In detail, the local contrast $c(x, y)$ is defined as follows:

$$c(x, y) = \frac{|p - a|}{|p + a|} \tag{10}$$

where p and a are the average values of pixels within a 3×3 region and a 7×7 surrounding neighborhood respectively . The performance measure of contrast improvement ratio, i.e., CIR, is defined as the ratio of the enhanced image and un-enhanced image within the region of interest R (ROI)

$$c(x, y) = \frac{\sum_{(x,y)\in R} |c(x, y) - \tilde{c}(x, y)|^2}{\sum_{(x,y)\in R} c(x, y)^2} \tag{11}$$

where c and $\tilde{c}$ are the local contrast values of original and enhanced images, respectively. In our experiment, we assume that R is the whole image.

For the objective evaluation of the contrast improvement, the proposed method was compared with three conventional enhancement methods such as the contrast stretching (CS), adaptive contrast enhancement (ACE), contrast gain transform (CGT) [13] and the method currently used in Macktype, a commercial software product [14]. We have tested 10 chromosome spread images and list the corresponding CIRs in Table 2. Our method consistently gives the highest CIRs among the five methods evaluated.

Image	CS	ACE	CGT	Macktype	Wavelets
case 1	.0868	.3487	.1874	0.2016	3.6877
case 2	.0270	.0435	.1440	0.6257	4.0704
case 3	.0246	.5017	.3183	0.7224	4.4152
case 4	.0230	.0523	.3163	0.7339	3.4430
case 5	.0233	.0753	.3221	0.6828	4.1676
case 6	.0276	.0369	.2849	0.5132	2.7958
case 7	.0275	.0755	.2389	0.4831	2.9241
case 8	.0244	.0470	.3092	0.7012	5.0110
case 9	.0311	.0371	.2345	0.4895	2.1790
case 10	.0151	.1257	.4973	1.7959	7.1507
Average	.0310	.1344	.2853	0.6949	3.9845

Table 2. A comparison of the CIRs for different methods.

5. DISCUSSIONS AND CONCLUSIONS

In this paper, we apply a class of differential wavelets [3] to image enhancement. The proposed wavelets have several advantages. First, they are derived from splines and can be implemented efficiently. Secondly, this class of representations are shift-invariant and thus facilitate the measurement of correlations of image features in these domains. In addition, these representations characterize the high-frequency edge information along horizontal, vertical and diagonal directions. We can take into account the directional information in designing the enhancement algorithms.

Our enhancement algorithm actually makes use of the information in the differential wavelet domains for extrapolation. Due to such wavelet representations, high frequency features such as edges are well characterized. Therefore, we can design our algorithm to enhance the images. Preliminary results show that our method significantly outperforms other conventional techniques in terms of the contrast improvement ratio. We plan to carry out human assessment of the enhancement performance of these images by clinicians in the near future.

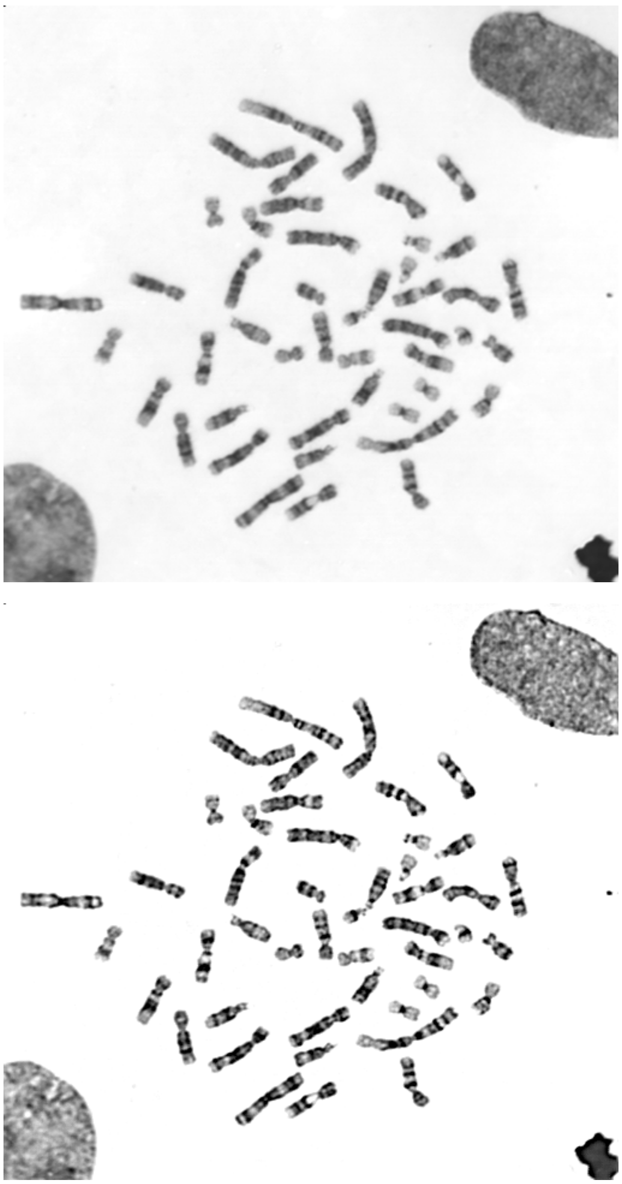

Fig. 2. An example of chromosome image enhancement. The original chromosome spread image is on the top and the enhanced result is on the bottom.

6. REFERENCES

[1] K. R. Castleman, *Digital image processing*, Prentice Hall, 1996.

[2] Yu-Ping Wang and S. L. Lee, "Scale-space derived from b-splines," *IEEE Trans. Pattern Anal. and Machine Intell.*, vol. 20, no. 10, pp. 1050–1065, Oct. 1998.

[3] Yu-Ping Wang, "Image representations using multiscale differential operators," *IEEE Trans. Image Processing*, vol. 8, no. 12, pp. 1757–1771, Dec. 1999.

[4] K. S. Song J. K. Kim, J. M. Park and H. W. Park, "Adaptive mammographic image enhancement using first derivative and local statistics," *IEEE Trans. Medical Imaging*, vol. 16, no. 5, pp. 495–502, Oct. 1997.

[5] C. H. Anderson H. Greenspan and S. Akber, "Image enhancement by nonlinear extrapolation in frequency space," *IEEE Trans. Image Processing*, vol. 9, no. 6, pp. 1035–1048, June 2000.

[6] Yu-Ping Wang and S. L. Lee, "From Gaussian scale-space to b-spline scale-space," in *Proceedings of ICASSP'99*, Phoenix, Arizona, March 15-19 1999, vol. 6, pp. pp.3441–3444.

[7] R. R. Coifman and D. L. Donoho, "Translation-invariant de-noising," in *Wavelets and Statistics*, A. Antoniadis and G. Oppenheim, Eds. Berlin: Springer-Verlag, 1995.

[8] B. M. Sadler and A. Swami, "Analysis of multiscale products for step detection and estimation," *IEEE Trans. Information Theory*, vol. 45, no. 3, pp. 1043–1051, April 1999.

[9] A. Rosenfeld, "A nonlinear edge detection technique," *Proc. IEEE.*, pp. 814–816, 1970.

[10] Y. Xu, B. Weaver, D. M. Healy, and J. Lu, "Wavelet domain filters: a spatial selective noise filtration technique," *IEEE Trans. Image Processing*, vol. 3, no. 11, pp. 747 –757, Nov. 1994.

[11] Yu-Ping Wang, S. L. Lee, and K. Torachi, "Multiscale curvature-based shape representation using b-spline wavelets," *IEEE Trans. Image Processing*, vol. 8, no. 11, pp. 1586–1592, Nov. 1999.

[12] R. Gordon and R. M. Rangayyan, "Feature enhancement of film mammograms using fixed and adaptive neighborhoods," *Applied Optics*, vol. 23, no. 4, pp. 560–564, 1984.

[13] D.-C. Chang and W.-R. Wu, "Image contrast enhancement based on a histogram transformation of local standard deviation," *IEEE Trans. Medical Imaging*, vol. 17, no. 4, pp. 518–531, 1998.

[14] *Macktype Software*, a trademark of Applied Imaging Corporation, 2000.